ELSEVIER

Shear of Structural Concrete Members and Pure Mode II Testing

Hans W. Reinhardt, Joško Ožbolt, Shilang Xu, and Abebe Dinku
Institute of Construction Materials, Stuttgart University, Stuttgart, Germany

The analysis of concrete members under shear action requires reliable material parameters. A new testing method has been developed which yields pure mode II. This has been demonstrated by numerical analysis as well as by analytical treatment. Tests have been performed on a high strength concrete (cylinder compressive strength of 85 MPa) which confirm the theoretical predictions. It is discussed how the new achievements can be used in predicting a size effect in concrete members under shear action. ADVANCED CEMENT BASED MATERIALS, 1997, 5, 75–85. © *1997 Elsevier Science Ltd.*

KEY WORDS: Concrete, shear, fracture mechanics, FE analysis, testing

On a macro scale, that is, when a structural engineer analyses a structural member, it is quite common to distinguish between normal forces, bending moments and shear forces, and to reinforce concrete accordingly. As bending shear is concerned, a part of the shear force is taken by the concrete compression zone, another by the stirrups, a third by the dowel action of the longitudinal reinforcement, and a fourth by the aggregate interlock in the crack. All sections of a structure are checked and reinforced according to the shear action. In such an approach, equilibrium of outer and inner forces has to be reached and compatibility of displacements has to be satisfied.

In a plain uncracked concrete section, the shear stress must be lower than an allowable shear stress which follows from a strength criterion, for instance, from the Mohr-Coulomb failure envelope. The same approach is followed for the calculation of the anchorage length of a reinforcing bar in concrete. Another loading case is the concentrated load on a small bearing area which is usually considered as a compression problem. However, the loading capacity is governed by the tensile behavior and, after cracking, a sliding motion occurs under the loading punch.

Address correspondence to: Hans W. Reinhardt, Institute of Construction Materials, Stuttgart University, Stuttgart, Germany.
Received April 24, 1996; Accepted September 12, 1996.

ISSN 1065-7355/97/$17.00
PII S1065-7355(96)00003-X

Looking closer to shear there are three stages involved: (1) as long as the concrete is uncracked there are two principal normal stresses (plane stress condition); (2) a crack forms perpendicular to the principal tensile stress direction; and (3) a sliding motion introduces shear along the crack faces. In terms of fracture mechanics, there is always a strong K_I and a weak K_{II} in the beginning. With crack extension and redistribution of stresses, however, mode II becomes more important on a lower stress level.

There are exceptions where mode II prevails right from the beginning. These are joints between dissimilar media under shear forces and normal forces parallel to existing cracks. For these cases a pure mode II testing should be available.

Mode II Testing Methods

Testing Methods Used

Some testing methods have been proposed and applied to various materials. Figure 1 shows eight specimen geometries and loading configurations which have been also applied to concrete. Figure 1a indicates the situation of pure shear stresses along a crack which is envisaged by testing but cannot be realized.

Figure 1b goes back to Iosipescu [1] who proposed this geometry for testing of metals and welded joints. It looks very attractive and has been used by several researchers on concrete either with a single notch specimen or a double notch specimen [2,3,4,5]. The results and interpretations were rather controversial. After Barr and Derradj [6], Schlangen [7] came to the conclusion that mode I is the governing mode of this test. The push-off specimen of Figure 1c was proposed by Mattock and Hawkins [8] to investigate interfaces in reinforced concrete. Finite element analyses have shown that a tensile stress exists at the crack tip, which is of the same magnitude as the shear stress, that is, a mixed state of stress exists. A variation of the same idea has been realized by Nooru-Mohamed [9]. The axisymmetric punch-through specimen (Figure 1d) has been analyzed by Tada [10]. It has been used on mortar and concrete [11] due to its easy handling. However, nu-

Advn Cem Bas Mat
1997;5:75–85

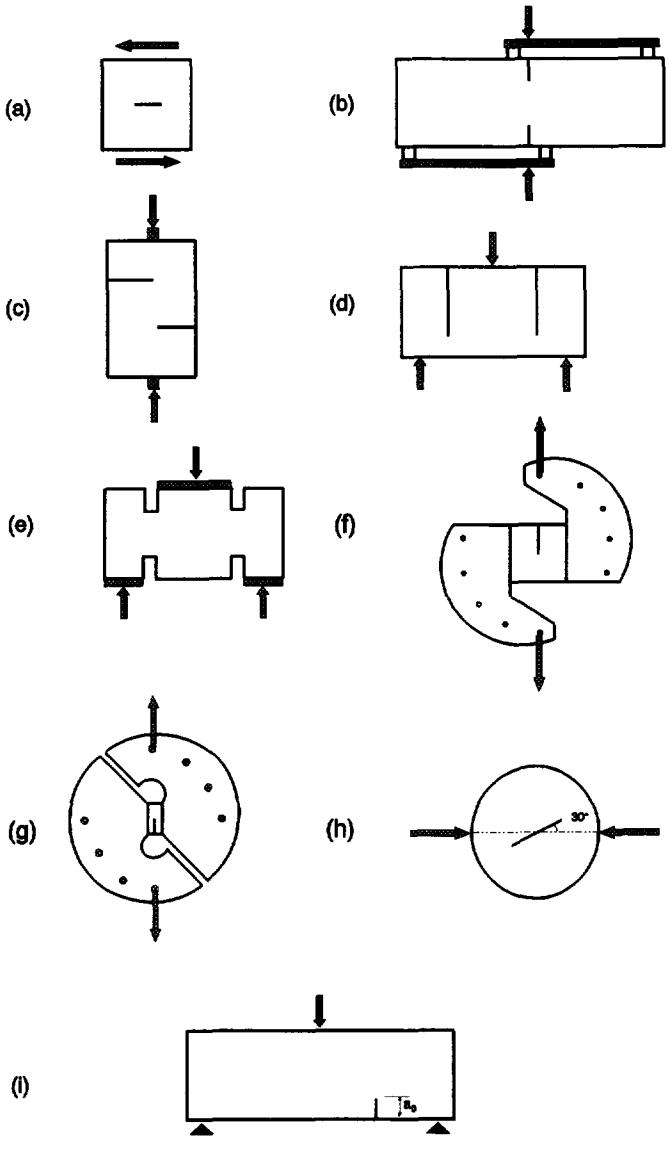

FIGURE 1. Different mode-II test configurations: (a) Schematic state of shear stresses along a crack; (b) Iosipescu specimen; (c) Push-off specimen; (d) Punch-through specimen; (e) Four-notch cylinder; (f) Mixed-mode device according to Richard; (g) Mixed-mode device according to Arcan; (h) Mixed-mode disk loading; and (i) Off-center notched beam.

merical studies have shown that large tensile stresses occur at the crack tip. A recent study has shown that the tensile stresses can be reduced considerably by choosing four notches instead of two and by varying the depth of the notches [12]. For rock core testing, the cylindrical specimen with four notches (Figure 1e) has been proposed by Luong [13] which yields mixed mode results. Figures 1f and 1g show elaborate testing devices which allow various mixed mode combinations by rotating the holder of the specimen. Both devices (Figure 1f, according to Richard [14], Figure 1g, according to Arcan [15]) were used in photo-elastic studies but not on concrete. Izumi et al. [16] have converted the device for compressive loading and applied to concrete in mixed mode loading. Due to compressive loading there is a negative K_I at the crack tip. Figure 1h has been proposed by Irobe and Pen [17] and also used by Jia et al. [18]. Finally, the off-center notched beam specimen by Jenq and Shah [19] has been applied in a study on mixed mode fracture (Figure 1i).

Although there are several methods proposed for mode II testing, none of them produces a pure mode II situation. Either by eccentric loading or by deformation during testing, a mode I contribution cannot be avoided which makes these testing arrangements mixed mode devices.

The Double-Edge Notched Infinite Plate

The continuing discussion about the existence of a pure shear fracture of concrete was the reason to look for an improved testing method. The double-edge notched plate seems appropriate. Figure 2 shows the geometry of a double-edge notched infinite plate under in-plane tensile loading. The ligament length is $2a$. Tada's [10] elastic solution yields to:

$$K_{II} = \frac{\sigma}{4}(\pi a)^{1/2}. \tag{1}$$

It is important to notice that K_I vanishes and K_{II} remains as the only stress component. This theoretical solution is valid for an infinite plate and the question is whether it is also applicable to a specimen of finite size.

The Double-Edge Notched Plate of Finite Size

The finite plate (see Figure 3) can be analyzed using the J-integral method [20]. To this end, the infinite strip of width $2w$ is cut into two halves (Figure 3b). The stress distribution along the axis of symmetry is assumed to be linear. The J integral, according to Radaj and Zhang [21], is expressed as:

$$J = \int_{\Gamma}(\tau_{xy}du + \sigma_y dv - Wdy) \tag{2}$$

with

$$W = \frac{1}{2E}[\sigma_x^2 + \sigma_y^2 - 2\nu\sigma_x\sigma_y + 2(1+\nu)\tau_{xy}^2]. \tag{3}$$

The stress intensity factors follow from

$$K_{II}^2 = JE \quad and \quad K_I = 0. \tag{4}$$

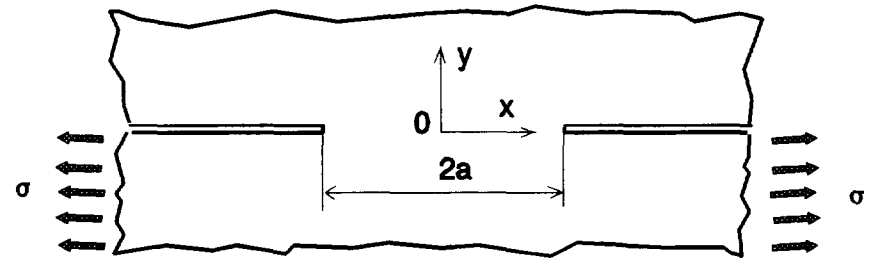

Fig. 2

a)

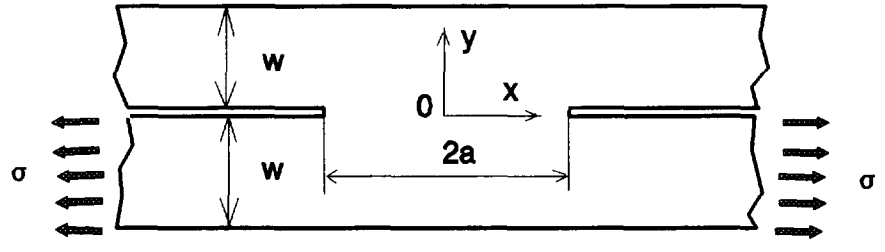

b)

FIGURE 2. Double-edge notched infinite plate.

Evaluating the integral along the path AB, BC . . . FG, GA it has been shown [22] that

$$K_{II} = \frac{\sigma}{4} w^{1/2} \tag{5}$$

The same result has been achieved by various authors [23,24,25,26] who used other mathematical tools when they analyzed the contact problem of two perfectly bonded infinite strips of dissimilar materials. The special case of the two equal materials and same width

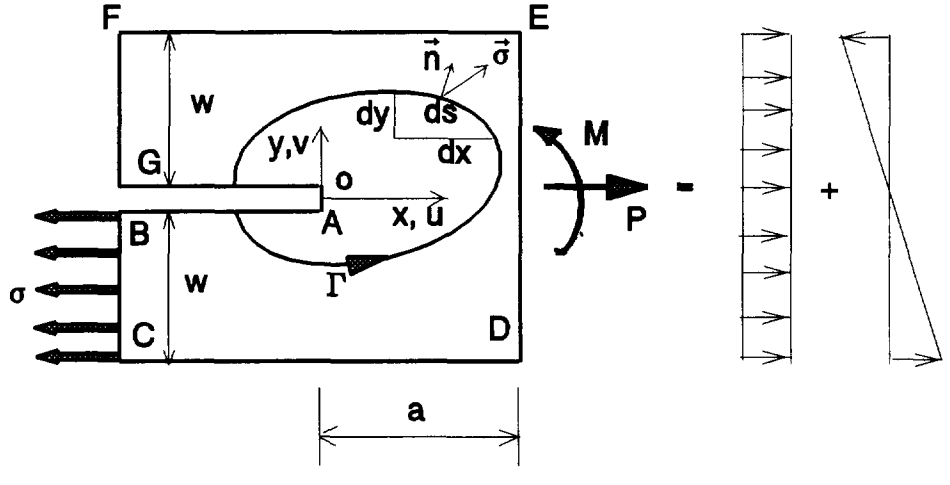

FIGURE 3. Double-edge notched infinite strip: (a) Geometry and (b) Integration path and loading.

Advn Cem Bas Mat
1997;5:75–85

leads to eq. (5) and $K_I = 0$. From [24] it is concluded that a finite length of the strip $h \geq 2a$ can be assumed to be infinite. Using this knowledge, a new specimen geometry for pure shear testing can be designed. The length of the specimen h should be $\geq 2a$ in order to apply eq. (5). Furthermore, for $h \geq 2a$ and $w \geq \pi a$ eq. (1) applies.

Predicted Size Effect

Equations (1) and (5) are suited to predict a size effect. According to eq. (1), K_{II} increases with $a^{1/2}$, that is, if the ligament ($2a$) of one structure is twice the one of another structure, the stress needed to reach K_{IIc} is only $(1/2)^{1/2}$ as large. Figure 4 shows the relation between ligament and critical stress. This relation applies to an infinite plate.

On the other hand, if the infinite plate is reduced to an infinite strip with finite width $2w$, eq. (5) does not show a dependence of the critical stress on the ligament length but only on the strip width. This means that the critical stress is constant for a constant w and varying ligament length. This is true until $w \leq \pi a$. Figure 5 shows the critical stress versus the ligament length for different strip widths.

The transition point shifts to the left with smaller width of the strip. Figure 5 shows that a size effect of the ligament length does only exist if $a \leq w/\pi$ (stable crack growth). The same have been shown by Ožbolt [27] for mode-I and mixed failure modes. Therefore, when judging a certain structure, the starting point in Figure 5 can lie on the curved line or on the horizontal line depending upon the combination of a and w.

There is a second feature of the double-edge notched plate which should receive attention. Equations (1) and (5) predict a critical stress for a certain K_{IIc}. If $K_{II} = K_{IIc}$ the crack (notch) will extend and, thus, the ligament length will decrease. As a consequence, the critical stress increases what means that $\sigma < \sigma_c$ and the situation is stable again. Figure 5 and eq. (5) predict that a crack will propagate until $a \leq w/\pi$ and that the crack arrests if the remote stress is kept constant. The crack propagates again only if the stress increases. This may lead to the situation that final shear failure will not occur but that other mechanisms govern the collapse, for instance, compressive failure.

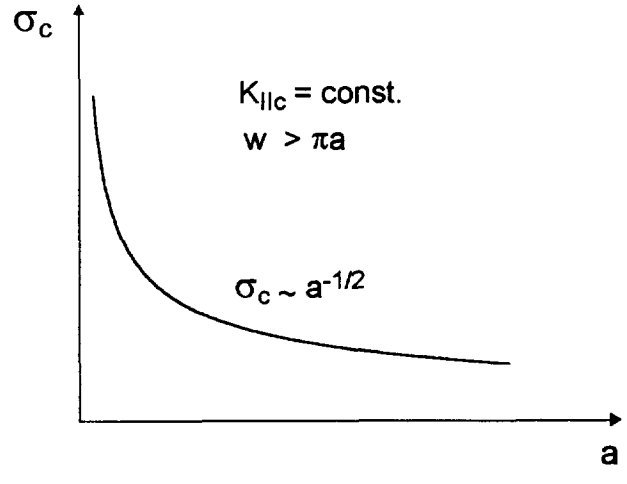

FIGURE 4. Influence of ligament length on critical stress.

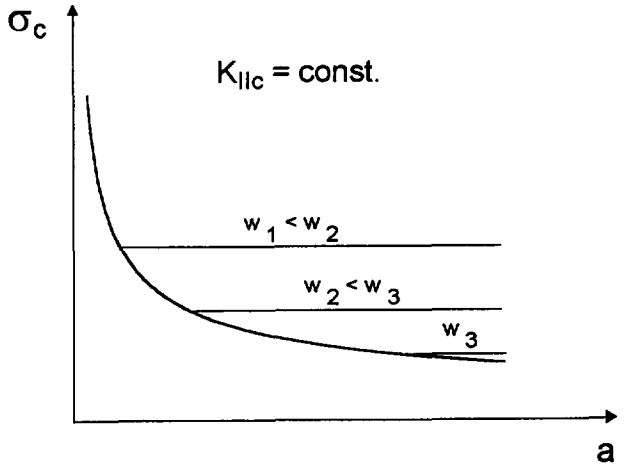

FIGURE 5. Critical stress versus ligament length and strip width.

Mode II Testing

In order to measure K_{IIc}, experiments on double-edge notched concrete test specimens (see Figure 6) have

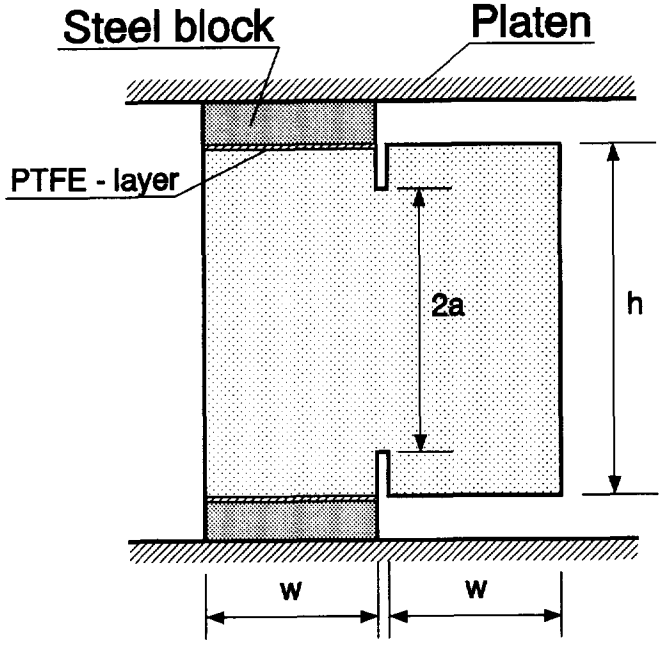

FIGURE 6. Geometry of the test specimen.

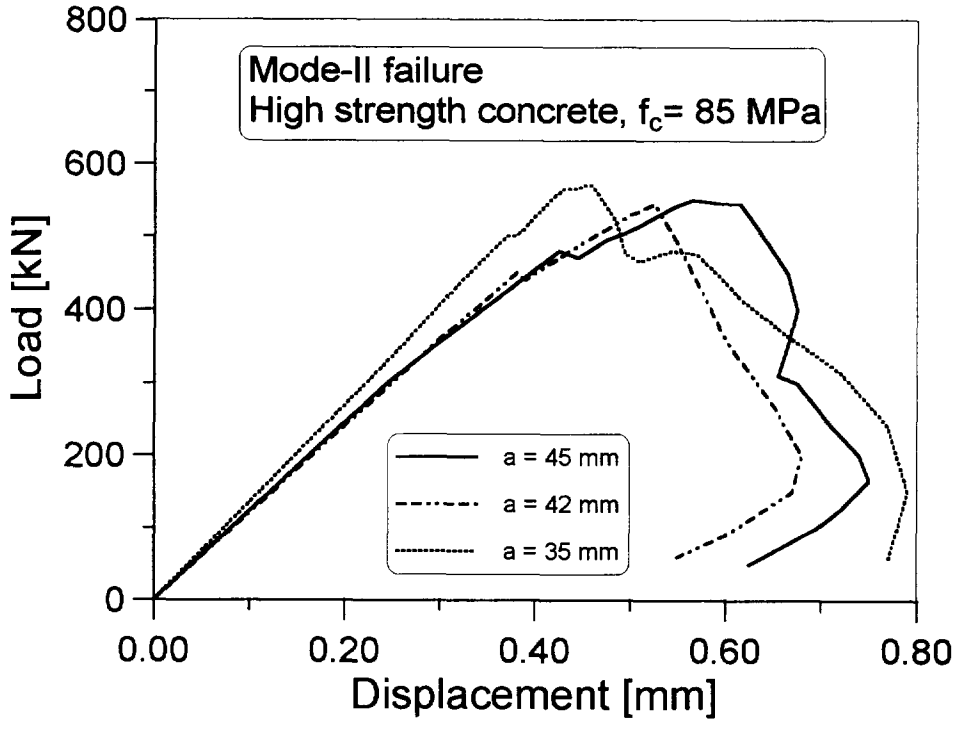

FIGURE 7. Measured load-displacement curves for a = 30, 42, and 45 mm.

been carried out. The new testing method is called double-edge notched compression test (DENCT). The dimensions of the specimens were 150 × 150 × 100 mm (h = 150 mm, w = 73 mm) with three different ligament lengths: a = 35, 42, and 45 mm. The width of the notch was constant and equal to 4 mm. The test specimens were made of high strength concrete with a maximum aggregate size of d_a = 16 mm. The average uniaxial compressive strength was f_c = 85 MPa and the mean tensile strength, as measured by splitting tests, was f_t = 5.0 MPa. To generate pure mode-II failure, one side of the specimen is loaded in compression by controlling the displacement of the loading platens. In order to eliminate the friction between the loading platens and concrete surface, the load is introduced through a layer of PTFE.

Measured load-displacement curves are plotted in Figure 7. A linear force-displacement relation follows until shortly before a kink in the line is observed. This discontinuity is caused by the formation and propagation of the first mode-II crack. The compressive stress at this point is called critical stress σ_c. The force increases again while the two mode-II cracks extend and new cracks are generated in the compressed part of the specimen. Finally, at ultimate compressive stress σ_u, the specimens fail by vertical splitting or diagonal shear. All specimens have been observed by a high resolution camera and the crack development has been recorded. Table 1 shows the ultimate compressive stresses (σ_u), the critical compressive stresses (σ_c), and calculated values for critical stress intensity factors (K_{IIc}). The critical stress intensity factors are calculated from measured σ_c using eq. (5) ($a > w/\pi$). As may be seen from Table 1, K_{IIc}, as well as σ_c, are approximately constant and independent of the ligament length.

Theoretically, the ultimate compressive stress should be independent on the ligament length. Namely, as soon as the mode-II crack starts it should propagate in a stable manner until the uniaxial compressive strength of concrete is reached. However, due to the inhomogeneity of concrete, shortly after mode-II crack initiation diagonal shear bands form which cause failure of concrete in compression before the mode-II crack extends to its full size. As a consequence, the fracture energy for mode-II failure cannot be measured. The ultimate compressive stress reaches maximum value for a = 0 and it is equal to the uniaxial compressive strength of concrete. When the ligament length increases, the ultimate compressive stress decreases. It approaches the theoretical minimum for $2a = h$ (unnotched specimen). This is explained by the fact that stronger localization of damage at the notch tip occurs on specimens with larger ligaments that causes an earlier (shear) compression failure.

TABLE 1. Mode II failure, experimental results, f_c = 85 MPa

a [mm]	σ_u [MPa]	σ_c [MPa]	K_{IIc} [MPa $\sqrt{m}$]
35	77.7	68.5	4.63
42	74.4	61.6	4.16
45	74.7	65.1	4.40

Advn Cem Bas Mat
1997;5:75–85

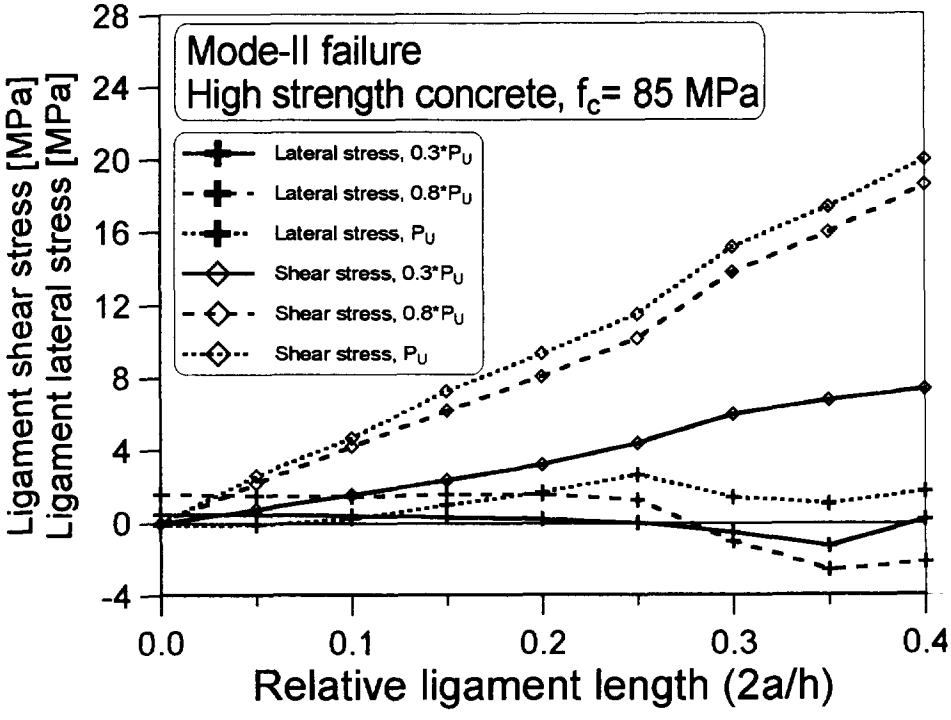

FIGURE 8. Distribution of the lateral and shear stresses over the ligament length for a = 30 mm at 30%, 80%, and 100% of ultimate load (hardening).

Numerical Study

To support and to confirm the experimental results, a numerical analysis has been carried out. The concrete properties used in the analysis were the same as in the experiments (f_c = 85 MPa, f_t = 5 MPa, G_f = 80 N/m, d_a = 16 mm, and Young's modulus E = 30000 MPa). In contrast to the experiments, in the numerical study, the ligament length was varied as a = 15, 30, 45, and 60 mm. The analysis is carried out using a nonlocal plane strain finite element (FE) code based on the microplane material model for concrete [28].

To demonstrate that the double-edge notched geometry generate a pure mode-II failure, in Figure 8 is the distribution of nodal lateral (σ_{xx}) and shear (σ_{xy}) stresses plotted over the half of the ligament length (vertical cross-section) for specimen with a = 30 mm. The stresses are shown at 30%, 80%, and 100% of the ultimate load. Independent of the load level, the lateral stresses over the vertical mid-plane ligament section are close to zero. Actually, zero values lie not exactly on the vertical mid-plane but somewhere inside the notch width, that is, zero lateral stress plane is not exactly vertical (plane). The exact position of zero lateral

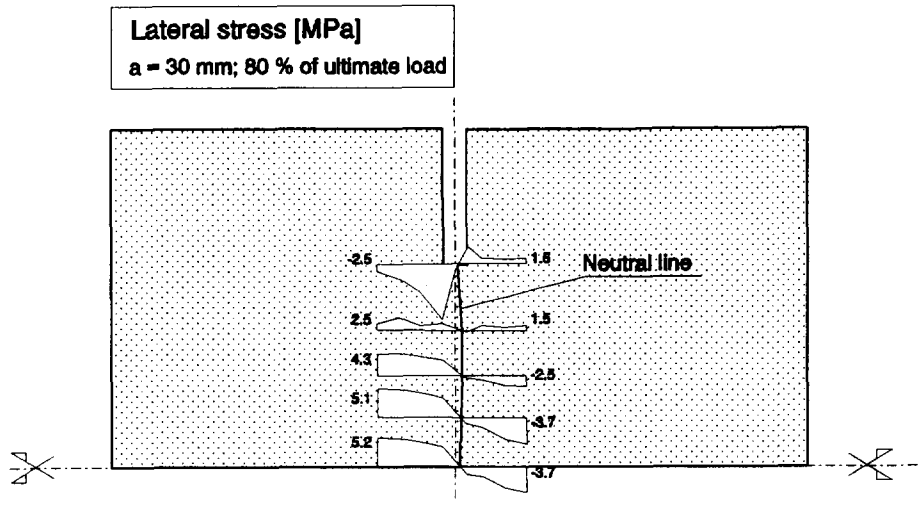

FIGURE 9. Position of the zero lateral stresses over the ligament length for a = 30 mm at 80% of ultimate load.

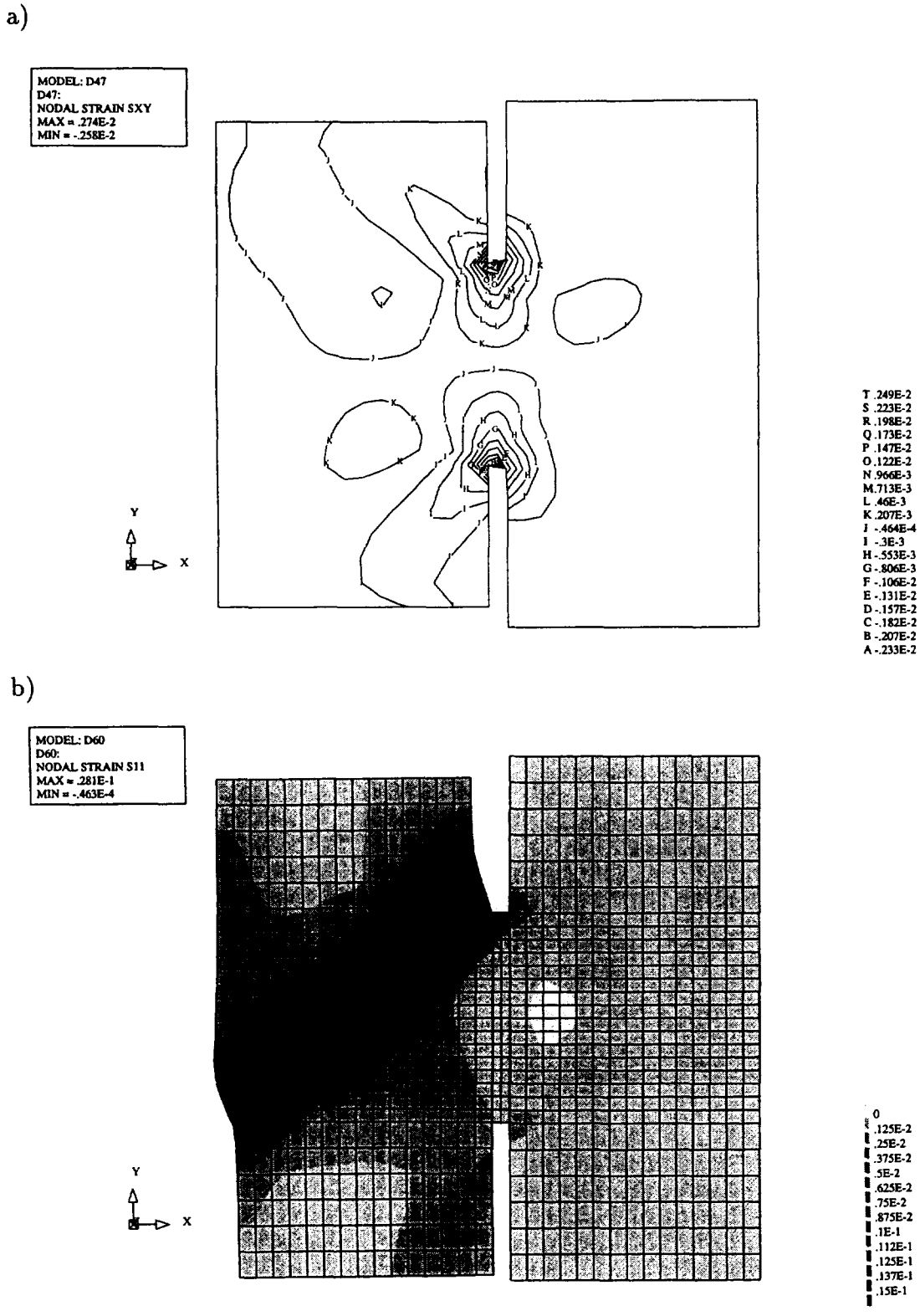

FIGURE 10. Strain fields for the specimen with a = 30 mm at: (a) initialization of the mode-II crack (approximately 80% of ultimate load—shear strains) and (b) in-post peak regime (diagonal shear failure—principle strains).

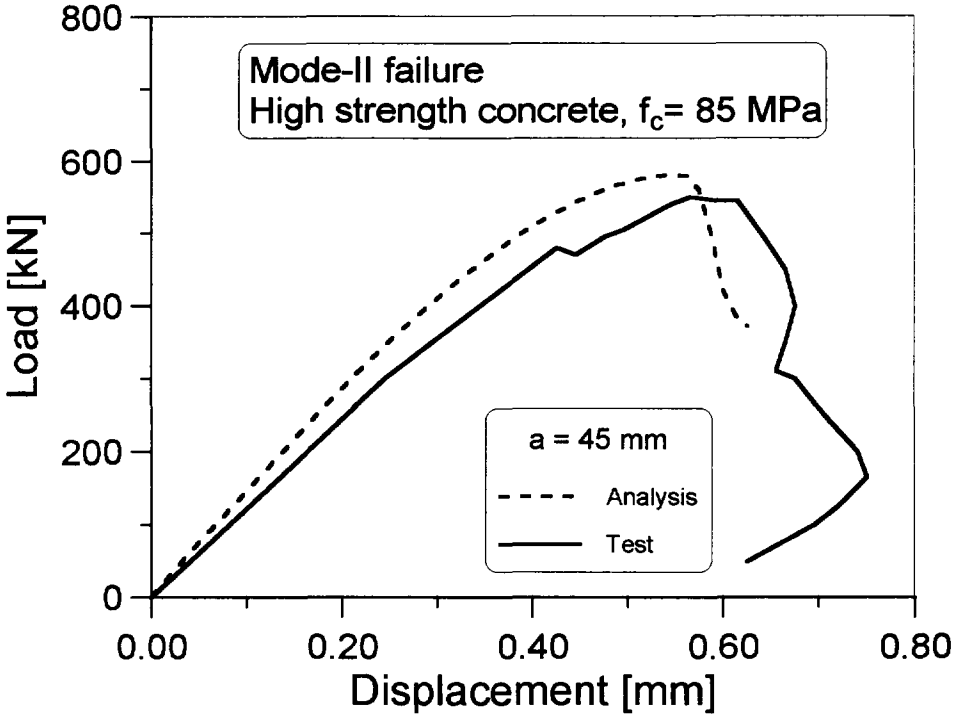

FIGURE 11. Load-displacement curves obtained in numerical analysis and measured in experiments for a = 45 mm.

stresses over the ligament length at 80% of ultimate load is plotted in Figure 9. The figure shows the distribution of the lateral stresses over the horizontal planes at different positions of the ligament. It proves that for double-edge notched test specimen we have a pure mode-II failure condition. Figures 10a and 10b show the principal strain patterns for the specimen with a = 30 mm plotted at 80% of the ultimate load (approximately initiation of the mode-II crack) and in the post-peak regime, closely before compression failure. The dark zones indicate the localization of damage in the form of the total principal strains. As can be seen, Figure 10b shows a typical diagonal shear failure in compression.

Figure 11 shows the calculated load-displacement curve plotted for a specimen with a = 45 mm. For comparison, in the same figure, the experimentally measured curve is also plotted. As may be seen, the agreement between numerical and experimental results is good.

Similar to experimental results, the numerical analysis shows that the specimens always fail in compression. Calculated ultimate stresses (see Table 2) decrease when the ligament length increases. Before compressive failure occurs, mode-II crack initiates. However, closely after its initiation mode-II crack growth is arrested and, instead, more critical diagonal shear failure in compression is initiated. To estimate the compressive stress at which mode-II crack initiates, the distribution of shear stresses at the notch tip is plotted as a function of the compressive stress for each geometry. For illustration, Figure 12 shows this plot for specimen with a = 30 mm. As one can see, for compressive stress of approximately $0.75 f_c$, the shear stress at the notch tip reaches the maximum (critical) value, that is, by further loading the shear stress remain approximately constant. Performing the above procedure for each ligament length we obtain critical shear stresses and corresponding critical compressive stresses. These values are summarized in Table 2.

In Figure 13 the critical shear stresses are plotted as a function of the relative ligament length. As may be seen for $0.3h < a < 0.7h$, the critical shear stress is approxi-

TABLE 2. Mode-II failure, numerical results, f_c = 85 MPa

a [mm]	σ_u [MPa]	τ_c [MPa]	σ_c [MPa]	K_{IIc} [MPa$\sqrt{m}$]	
15	82.2	15.5	81.5	4.42	N.A.
30	81.0	20.5	68.6	N.A.	4.63
45	77.5	22.5	61.8	N.A.	4.17
60	76.2	28.0	63.9	N.A.	4.32

N.A. = not applicable.

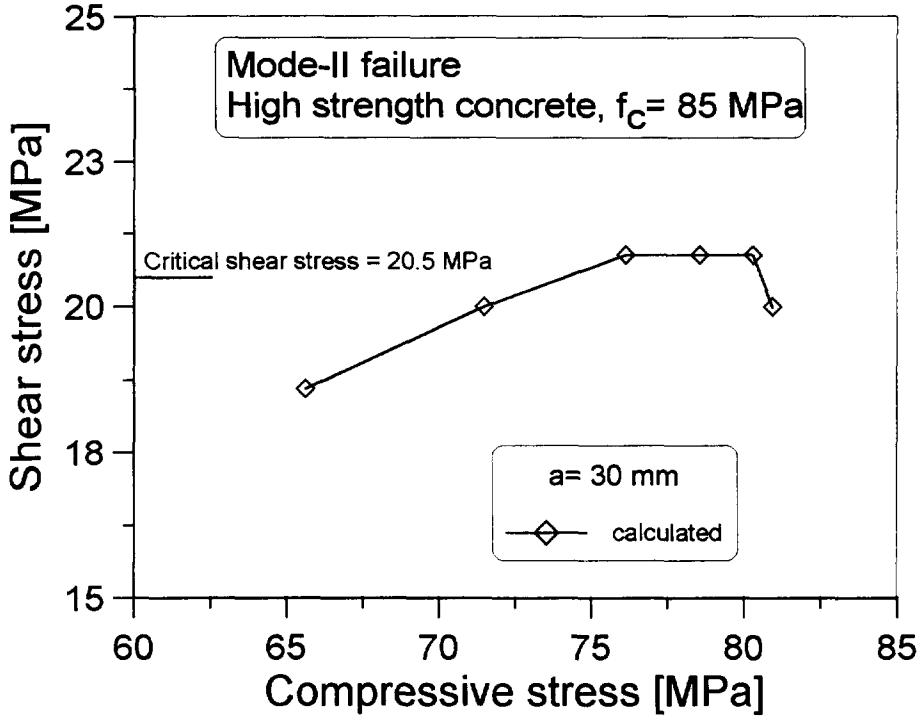

FIGURE 12. Shear stresses at the notch front as a function of the compressive stress obtained from the numerical study for a = 30 mm.

mately constant and in average τ_c = 21.5 MPa. For $a/h <$ 0.3, the critical shear stress tends to zero, that is, if the ligament length is too short (less than approximately maximum aggregate size), mode-II failure cannot be realized since the stress-strain distribution is close to be uniform (uniaxial compression). On the contrary, if the ligament length is larger than $0.7h$, the critical shear strength tends to increase. The reason is due to the fact that the notch tip is too close to the concrete loading surface and therefore the influence of the boundaries is too strong.

Based on the results shown in Table 2, from known critical compressive stresses, K_{IIc} values are calculated using Tada's formula for $a < w/\pi$ and eq. (5) for $a > w/\pi$

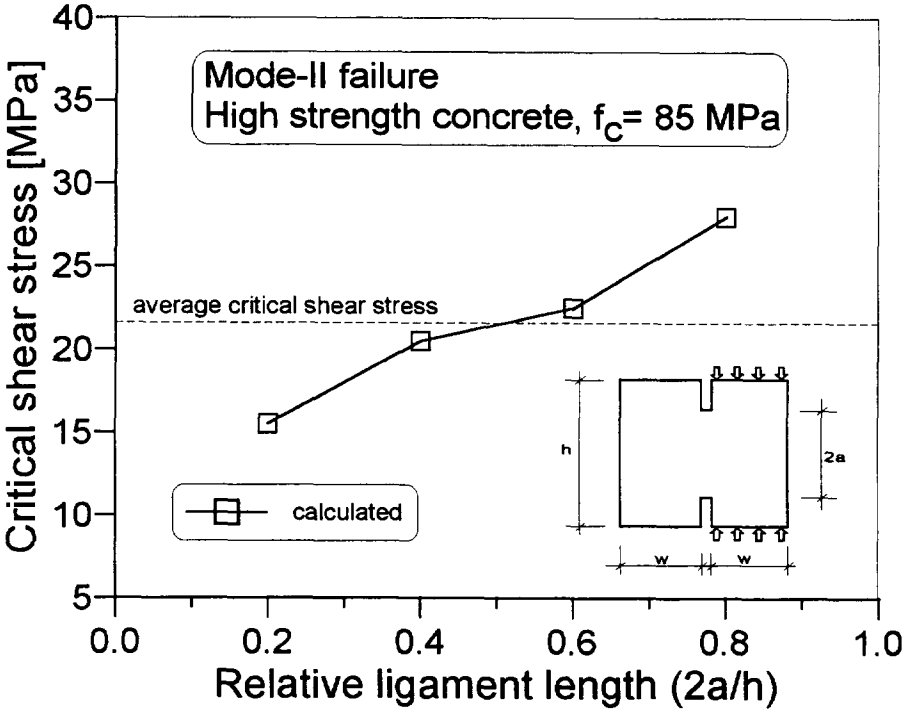

FIGURE 13. Critical shear stress as a function of the relative ligament length obtained in the numerical analysis.

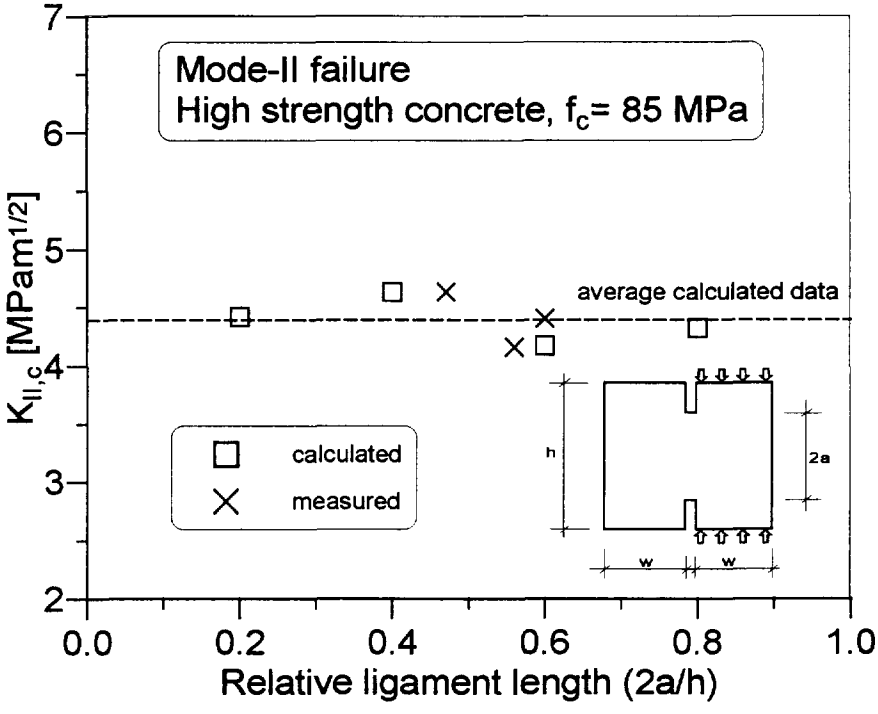

FIGURE 14. Critical K_{II} obtained using eq. (1) or eq. (5), respectively,—numerical and experimental results.

(see Table 2) and plotted in Figure 14 as a function of the relative ligament length. As may be seen, although the critical shear stress is not constant K_{IIc}, as well as σ_c for $a > w/\pi$ are approximately constant (see Figure 13), that is, independent on the ligament length. The average calculated value obtained in the numerical analysis is 4.39 MPa $\sqrt{m}$. For comparison, in the same figure, the test results are also shown. As one can see, the agreement is good. Figure 14 confirms that for the present geometry, Tada's formula and eq. (5) give a good estimation of K_{IIc}. Namely, K_{IIc} values were calculated based on the critical compressive stresses which correspond to the critical shear stresses obtained from the numerical study.

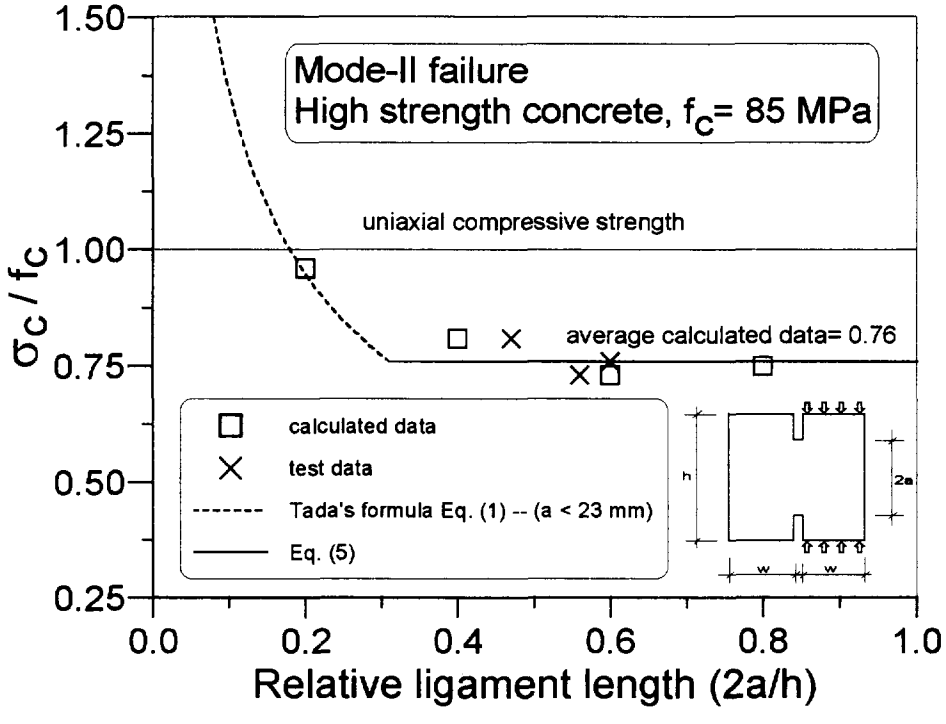

FIGURE 15. Critical compressive stress as a function of the relative ligament length—numerical and test results compared with eq. (1) and eq. (5), respectively, under the assumption that for $a > w/\pi$ σ_c/f_c = 0.76 (average calculated data).

In Figure 15 the relative critical compression stresses are plotted as a function of the relative ligament length. Calculated and test data are compared with the predictions of Tada's formula eq. (1) and eq. (5), assuming that for $a = w/\pi$ σ_c = average calculated value from the numerical study ($\sigma_c = 0.76 f_c$ = 64.6 MPa). Figure 15 shows that for $a > w/\pi$, the critical compressive stress is approximately constant, that is, independent of the ligament length. This is in agreement with the theoretical prediction (see eq. 5). However, for $a < w/\pi$, the critical compressive stress increases what is again in agreement with the theoretical prediction based on Tada's formula. For $a \leq h/10$, the critical compressive stress approximately coincides with the uniaxial compressive strength. Numerical results, test results, as well as theoretical predictions, are in agreement. The study indicates that for $a > w/\pi$, the critical compressive stress is reached at approximately $\sigma_c = 0.75 f_c$ and for this test series $K_{IIc} = f_c/19$ with K_{IIc} in MPa $\sqrt{m}$ and f_c in MPa. Whether this relation is true for other concrete strengths has to be confirmed by further experiments.

Discussion of the Results

According to our knowledge, at present, there is no test method which is able to generate a pure mode-II failure. Most test setups generate so-called mixed mode failures. The present tests and numerical results, using double-edge notched specimen, generate during the entire load history pure mode-II conditions. Due to the inhomogeneity of concrete, after mode-II crack initiation, its further propagation is arrested and overidden by more critical diagonal shear failure in compression. Consequently, mode-II fracture energy in experiments, as well as in the analysis, could not be measured. However, the critical stress intensity factor can be simply obtained.

The measured and calculated values exhibit good agreement. The present study has yielded K_{IIc} values which are in good agreement with values estimated from other researches [4,15]. The average calculated value for K_{IIc} was 4.38 while the average test data was almost the same and equal to 4.40 MPa$\sqrt{m}$.

The critical stress intensity factor K_{Ic} may be in the order of 1 MPa$\sqrt{m}$ which is about one fifth of K_{IIc}. If we assume that fracture energy G_f is proportional to the critical energy release rate G_c, and since $K = \sqrt{GE}$, it would mean that $G_{II,f}$ is about 25 times as large as $G_{I,f}$.

Conclusions

The analytical and numerical studies have demonstrated the validity of the new testing method for pure Mode II. Tests on high strength concrete agreed with the theoretical prediction. It is now feasible to determine material properties which are needed for a reliable analytical or numerical analysis of shear problems of beams and slabs.

Furthermore, the analytical formula, as well as numerical results for the double-edge notched strip, predicts that the size effect depends on the geometry. Equation (5) is valid for narrow strips whereas eq. (1) applies for wide strips. Figures 5 and 15 demonstrate clearly that situations with and without a size effect occur depending on the geometry.

References

1. Iosipescu, N. *J Mater.* **1967,** *2,* 537–566.
2. Arrea, M.; Ingraffea, A.R. *Mixed-Mode Crack Propagation in Mortar and Concrete.* Department of Structural Engineering Report 81–13, Cornell University: New York, 1981.
3. Bažant, Z.P.; Pfeiffer, P.A. *Mater. & Struct. (RILEM),* **1986,** *110,* 111–121.
4. Swartz, S.E.; Taha, N.M. *Eng. Fract. Mech.* **1990,** *35,* 137–144.
5. Ballatore, E.; Carpinteri, A.; Ferrara, G. *Eng. Fract. Mech.* **1990,** *35,* 145–157.
6. Barr, B.; Derradj, M. *Eng. Fract. Mech.* **1990,** *35,* 171–180.
7. Schlangen, E. *HERON* **1993,** *38.*
8. Mattock, A.H.; Hawkins, N.M. *PCI, J.* **1972,** March-April, 55–75.
9. Nooru-Mohamed, M.B. *Mixed-Mode Fracture of Concrete: An Experimental Approach,* Ph.D. thesis. Delft University of Technology: Delft, The Netherlands, 1992.
10. Tada, H.; Paris, P.; Irwin, G. *The Stress Analysis of Cracks Handbook, 2nd ed.* Paris Productions Incorporated: St. Louis, 1985.
11. Davies, J. In *Fracture Processes in Concrete, Rock and Ceramics* (RILEM Proceedings 13); van Mier, J.G.M.; Rots, J.A.; Bakker, A., Eds. E & FN Spon: London, 1991.
12. Davies, J. *Cem. Concr. Res.* **1995,** *25,* 1031–1042.
13. Luong, M.P. *Eng. Fract. Mech.* **1990,** *35,* 127–135.
14. Richard, H.A. *Int. J. Fract.* **1981,** *17,* R105–R107.
15. Banks-Sills, L.; Arcan, M. *Exp. Mech.,* **1983,** *Sept.,* 257–261.
16. Izumi, M.; Mihashi, H.; Numura, N. In *Fracture Toughness and Fracture Energy of Concrete;* Wittmann, F.H., Ed. Elsevier Science: Amsterdam, 1986; 347–354.
17. Irobe, M.; Pen, S.-Y. In *Fracture Mechanics of Concrete Structures;* Bažant, Z.P., Ed. Elsevier Science: London and New York, 1992; 719–726.
18. Jia, Z.; Shah, S.P. *Cem. Concr. Res.* **1996,** *26,* 125–137.
19. Jenq, Y.S.; Shah, S.P. *Int. J. Fract.* **1988,** *38,* 123–142.
20. Rice, J.R. *J. Appl. Mech.* **1968,** *35,* 379–386.
21. Radaj, D.; Zhang, S. *Eng. Fract. Mech.* **1991,** *39,* 391–413.
22. Xu, S.; Reinhardt, H.W.; Gappoev, M. *Int. J. Fract.* (in press).
23. Keer, L.M. *J. Appl. Mech.* **1974,** *Sept.,* 679–683.
24. Yahsi, O.S.; Göcmen, A.E. *Int. J. Fract.* **1987,** *34,* 162–177.
25. Keer, L.M.; Guo, Q. *Int. J. Fract.* **1990,** *43,* 69–81.
26. Keer, L.M.; Guo, Q. *Adv. Fract. Res.* **1989,** *4,* 3073–3080.
27. Ožbolt, J. *Maßstabseffekt und Duktilität von Beton- und Stahlbeton-konstruktionen.* Postdoctoral thesis. Stuttgart University: Stuttgart, Germany, 1995.
28. Ožbolt, J.; Bažant, Z.P. *Int. J. Num. Meth. Eng.* **1996,** *39,* 631–661.